



LJMU Research Online

Crandell, K, Howe, R and Falkingham, PL

Repeated evolution of drag reduction at the air-water interface in diving kingfishers

<http://researchonline.ljmu.ac.uk/id/eprint/10697/>

Article

Citation (please note it is advisable to refer to the publisher's version if you intend to cite from this work)

Crandell, K, Howe, R and Falkingham, PL (2019) Repeated evolution of drag reduction at the air-water interface in diving kingfishers. *Interface*, 16 (154). ISSN 1742-5689

LJMU has developed **LJMU Research Online** for users to access the research output of the University more effectively. Copyright © and Moral Rights for the papers on this site are retained by the individual authors and/or other copyright owners. Users may download and/or print one copy of any article(s) in LJMU Research Online to facilitate their private study or for non-commercial research. You may not engage in further distribution of the material or use it for any profit-making activities or any commercial gain.

The version presented here may differ from the published version or from the version of the record. Please see the repository URL above for details on accessing the published version and note that access may require a subscription.

For more information please contact researchonline@ljmu.ac.uk

<http://researchonline.ljmu.ac.uk/>

1
2
3 14
5 2 **Repeated evolution of drag reduction at the air-water interface**
6
7
8 3 **in diving kingfishers**
9

10 4

11
12 5 Crandell, KE*, Howe, RO*, Falkingham, PL **
13
14

15 6

16
17 7 * School of Natural Sciences, Bangor University
1819 8 ** School of Natural Sciences, Liverpool John Moores University
20
21

22 9

23
24 10 **ABSTRACT**25
26 11 Piscivorous birds have a unique suite of adaptations to forage under the water. One
27
28 12 method aerial birds use to catch fish is the plunge dive, wherein birds dive from a
29
30 13 height to overcome drag and buoyancy in the water. The kingfishers are a well-
31
32 14 known clade that contains both terrestrially foraging and plunge-diving species,
33
34 15 allowing us to test for morphological and performance differences between foraging
35
36 16 guilds in an evolutionary context. Diving species have narrower bills in the dorso-
37
38 17 ventral and sagittal plane and longer bills (size corrected data, n=71 species, p<0.01
39
40 18 for all), Although these differences are confounded by phylogeny (phylogenetically
41
42 19 corrected ANOVA for dorso-ventral p=0.26 and length p=0.14), beak width in the
43
44 20 sagittal plane remains statistically different (p<0.001). We examined the effects of
45
46 21 beak morphology on plunge performance by physically simulating dives with 3D
47
48 22 printed models of beaks coupled with an accelerometer, and through computational
49
50 23 fluid dynamics (CFD). From physically simulated dives of bill models, diving species
51
52
53
54
55
56
57
58
59
60

1
2
3 24 have lower peak decelerations, and thus, enter the water more quickly, than
4
5 25 terrestrial and mixed-foraging species (ANOVA $p=0.002$), and this result remains
6
7 26 unaffected by phylogeny (phylogenetically corrected ANOVA $p=0.05$). CFD analyses
8
9
10 27 confirm these trends in three representative species, and indicate that the
11
12 28 morphology between the beak and head is a key site for reducing drag in aquatic
13
14
15 29 species.
16
17
18
19
20
21
22
23
24
25
26

31 Keywords: plunge diving, avian hydrodynamics, beak, bow wave, *Alcedinidae*
32
33

34 INTRODUCTION

35

36 Plunge diving has evolved in multiple flying species to facilitate transitioning
37 between the air and water – two mediums of vastly different densities. Birds
38 including gannets, terns, and boobies have mastered diving from air into water to
39 access fish meters below the surface. Morphological adaptations likely compliment
40 this foraging strategy in order to both improve dive efficiency and avoid damage on
41 water entry. The shape of the kingfisher's bill has served as inspiration as a drag-
42 reducing structure for the Japanese Shinkansen Bullet train (1, 2). However, these
43 functions have yet to be directly tested.

44 The conversion of gravitational potential energy to kinetic energy during the
45 dive provides momentum for the bird to overcome body drag and buoyancy in order
46 to dive deeper (3). Birds are particularly buoyant due to the layer of air trapped

1
2
3 47 between the body and the feathers, typically used for insulation (4), as well as body
4
5 48 fat and the avian system of airsacs (5). In the diving species the Lesser Scaup
6
7
8 49 (presumably already adapted to reduce drag), over 80% of work during a dive is to
9
10 50 overcome the significant costs of body buoyancy (6).

11
12 51 Minimizing the energetic costs of drag have led to streamlined bauplans in
13
14 52 swimming and flying animals (7-11). Bird beaks appear well-adapted to avoid both
15
16 53 aerodynamic and hydrodynamic drag. Most beaks are relatively cone-shaped, with a
17
18
19 54 small initial surface area relative to the direction of oncoming flow – thus reducing
20
21 55 immediate profile drag. The gradual increase in cross-sectional area allows flow to
22
23
24 56 remain laminar as it travels toward the wide middle-section of the animal.

25
26 57 While much work has focused on how shape influences drag across flying
27
28 58 and swimming animals, less work exists examining morphological function at the
29
30 59 air-water interface. Diving involves the animal rapidly transitioning between two
31
32 60 fluids of different physical properties – from air, a relatively low density and
33
34
35 61 viscosity fluid, to water, a higher density and viscosity fluid. Due to the high speed of
36
37 62 entry, diving comes at the cost of an initial impact at the water's surface. Gannets
38
39
40 63 reportedly dive from a height of 30 meters in the air– a fall resulting in a speed of 22
41
42 64 m/s when impacting the water (3). While these impact speeds could seriously
43
44 65 damage a human entering feet-first (12), an avian injury due to water entry has not
45
46 66 been reported. The neck musculature coupled with streamlined beak and skull help
47
48
49 67 the gannet avoid injury by reducing impact forces (12). In fact, large decelerations
50
51 68 due to water impact during diving may not occur in birds. Accelerometers mounted
52
53
54 69 to free-living Cape Gannets sampling at 16 to 32 Hz detected no or minimal

1
2
3 70 deceleration due to impact during foraging dives. (3). Drag reduction due to
4
5 71 morphology may help reduce immediate impact forces. The hydrodynamic shape of
6
7 72 the avian bill may also reduce turbulence during the initial dive, which may help
8
9
10 73 avoid visual or vibrational detection by the prey (13).

11
12 74 Recent work examining water piercing by geometric cones suggests that
13
14 75 beak morphology may be selected on to reduce impact force, and thus, drag on entry
15
16 76 (14). The lower the opening angle of the cone (or the tip angle), the lower impact
17
18 77 forces and more smooth the transition between air and water (14). The opening
19
20 78 angle of a cone (α) can be calculated as $\alpha = 2 \cdot \arcsin(r/s)$, where r is the radius of the
21
22 79 base, and s is the length of the side from base to tip (also called 'slant height'). Thus,
23
24 80 to decrease the angle of a cone, either the radius of the base (r) must decrease, or
25
26 81 the length (s) must increase. If diving species of kingfisher are morphologically
27
28 82 adapted to minimize drag, we would expect them to have longer bills with a
29
30 83 narrower base relative to terrestrial species.

31
32 84 Kingfishers (Alcedinidae) are an ideal clade in which to explore
33
34 85 morphological adaptations for diving. They comprise 114 species that encompass
35
36 86 terrestrial, aquatic, and mixed (both terrestrial and aquatic) foraging strategies (15),
37
38 87 allowing us to test function and morphology in an evolutionary context. Here, we
39
40 88 examine beak morphology to elucidate patterns of streamlining in diving species.
41
42 89 We test hydrodynamic properties of bird beak shape by simulating dives with scaled
43
44 90 3D printed plastic models of the birds. Printed models allow us for the first time to
45
46 91 isolate shape from size. Lastly, we use Computational Fluid Dynamics to explore
47
48 92 flow around the beak and head.

1
2
3 934
5 94 **METHODS**6
7
8 959
10 96 *Morphometrics*11
12 97

13
14
15 98 3D digital models of bird beaks were generously provided by the Mark My
16
17 99 Bird project as 3D scans of specimens housed in the Natural History Museum at
18
19 100 Tring and the Manchester Museum (See Appendix 1 for museum details and
20
21 101 specimen IDs). Please see information in the appendix of (16) for details pertaining
22
23 102 to scanning methodologies. The scans are available for download by request from
24
25 103 markmybird.org. The scan of a Forest Kingfisher (*Todiramphus macleayii*) was
26
27 104 obtained from a specimen in the Bangor University Brambell Natural History
28
29 105 Museum. This scan was produced by Rowan Howe at the Pontio Innovation Centre
30
31 106 with an Artec Spider (Artec Group, Luxembourg), with a standard resolution of 0.05
32
33 107 mm and mesh resolution of 0.1 mm. Mesh generation was accomplished with Artec
34
35 108 Studio 9 (Artec Group, Luxembourg).

36
37
38 109 Morphometrics were measured directly from specimen scans, representing
39
40
41 110 71 species (Appendix 1; Figure 1). Beak width was measured as the linear distance
42
43 111 between either end of the lower and upper mandible external hinge. Beak height
44
45 112 was measured from the linear distance between the most dorsal and most ventral
46
47 113 points where the beak meets the feathered portion of the head along the sagittal
48
49 114 plane. Beak length was measured from the tip of the bill to the end of the mandible
50
51 115 hinge (Figure 2).

1
2
3 116 The mass of the individual museum specimen prior to preservation is
4
5 117 unknown. Body size from the literature was used as an estimation of representative
6
7 118 body size for each specimen. Masses for each species were found in the CRC
8
9 119 Handbook of Avian Masses (17). When available, average mass for a species was
10
11 120 used. If male and female mass was reported separately, the two were averaged for
12
13 121 subsequent analyses. Any species for which mass data was not available was
14
15 122 excluded from this study.
16
17
18
19

20 123

21
22 124 *3D model manufacturing*
23

24 125

25
26 126 Thirty-one species were subsampled for functional testing, representing a
27
28 127 variety of foraging strategies and body sizes across the kingfisher phylogeny (Figure
29
30 128 3). One beak model was printed for each of 31 species (Appendix 1).
31
32

33 129 Prior to 3D printing, scans were post-processed in Ultimaker Cura 3 to
34
35 130 remove holes. To account for differences in drag due to body size, all scans were
36
37 131 geometrically scaled to 9 cm from the tip to the posterior of the beak (Figure 2).
38
39 132 Scans were finished by a transverse cut across the head of the animal at the end of
40
41 133 the beak. This cut allowed us to incorporate the entire morphology of the beak
42
43 134 alongside the joint where the beak meets the head.
44
45

46
47 135 3D prints were produced on an Ultimaker 3+ (Ultimaker, Cambridge, MA,
48
49 136 USA) with a 0.4 mm nozzle size. Prints were produced with a layer height of 0.1 mm,
50
51 137 infill density of 20%, and four gradual infill steps. Beaks were printed with
52
53
54
55
56
57
58
59
60

1
2
3 138 biodegradable plastic poly lactic acid (PLA) filament (RS Components Ltd,
4
5 139 Northants, UK).

6
7
8 140

9
10 141 *Physically Simulated dives*

11
12 142

13
14
15 143 Beak models were attached to a closed 50 ml falcon conical centrifuge tube.

16
17 144 The models were mounted to a 9 cm long wooden or plastic dowel to increase the

18
19 145 distance between the beak and falcon tube 'dive body,' thus minimizing any effects

20
21 146 of the tube shape and buoyancy during the initial entry phase of the dive. The tube

22
23 147 contained an Axivity AX-3 triaxial accelerometer (Axivity Ltd, Newcastle, UK)

24
25 148 sampling at 1600 Hz with a maximum value of ± 16 G. The accelerometer was

26
27 149 oriented to the beak model with the negative x axis aligned with gravity, and the

28
29 150 positive z axis oriented dorsally. The falcon tube was weighted to equalize the

30
31 151 weight of every model and support beam to that of the largest model. The mass of

32
33 152 each of the total structure including models totaled 71.1 grams.

34
35 153 A fishing line track mounted perpendicular to the water surface was used to

36
37 154 maintain model orientation during the dive. The tube was fitted with plastic

38
39 155 drinking straws on either side lengthwise and threaded on to fishing line. The dive

40
41 156 tank was a 60 cm tall flower vase with an opening of 25 cm. (Figure 4A). A

42
43 157 simulated dive was performed by dropping the model (beak pointed down) in to the

44
45 158 tank along the fishing wire track from 75 cm above the surface of the water. To

46
47 159 confirm acceleration was not impacted by the trackway, and the accelerometer gave

1
2
3 160 a reliable reading, the accelerometer gravity axis during the fall was double
4
5 161 integrated, and resulted in the correct 75 cm.
6
7

8 162 The fishing line maintained orientation of the models vertically, although
9
10 163 slight differences in entry angle along the dorso-ventral plane were apparent,
11
12 164 leading to slight variation in deceleration values. To account for this, 10 drops were
13
14 165 performed for each model. All acceleration analyses were done only on the vertical
15
16 166 (orthogonal to the water surface) component. All accelerometer outputs were
17
18 167 analyzed in a custom written Matlab script. For the purposes of this study, only the
19
20 168 initial deceleration phase was analyzed – the time between when the beak has
21
22 169 entered the water and has become fully submerged. At the time of submergence, the
23
24 170 model experiences a maximum deceleration (Figure 4B).
25
26
27
28

29 171 Any outliers above 3 standard deviations were removed from subsequent
30
31 172 analyses. Resulting analyses for inter-species comparisons used the average
32
33 173 maximum deceleration for each model.
34
35

36 174

37
38 175 *Statistical analyses*
39

40
41 176 Each species was assigned to a foraging group based on behavior and diet
42
43 177 descriptions in the Handbook of Birds of the World Alive (18). Three foraging
44
45 178 groups were used: terrestrial, aquatic, or both. If a species could not be readily
46
47 179 assigned to one of these groups, it was not included in the study.
48
49

50 180 For analyses of morphological characters, in order to meet assumptions of
51
52 181 normality and homoscedasticity, all measurements were log-10 transformed prior
53
54 182 to analyses. Morphometric characters were tested for size-dependence with a linear
55
56
57
58
59
60

1
2
3 183 regression between character and reported body size (all $p < 0.01$). All three were
4
5 184 adjusted for size by regressing log-10 adjusted values against log-10 adjusted body
6
7
8 185 mass and calculating the residuals. The residuals were used for subsequent
9
10 186 comparisons. An analysis of variance (ANOVA) tested for differences between
11
12 187 foraging groups.

13
14
15 188 In order to account for phylogenetic effects, a phylogenetic tree was
16
17 189 constructed based on Anderson et al. (19) (Figure 1). Binomial names according to
18
19 190 the Jetz et al. (20) phylogeny were used. *Alcedo euryzona* was placed as sister taxa to
20
21 191 its conspecific *A. peninsulae* (18). To explore the relationship between foraging
22
23 192 guild and performance, a sub-sampled phylogeny of the 31 tested species was
24
25 193 constructed from the first phylogeny (Figure 3). These 31 species were selected to
26
27 194 encompass a range of foraging guilds and body sizes across the phylogeny. In both
28
29 195 phylogenies, branch lengths were set using arbitrary lengths using a Grafen
30
31 196 transformation (21). We tested for differences in morphology and hydrodynamic
32
33 197 function between foraging groups with a phylogenetically corrected ANOVA
34
35 198 according to Garland et al.'s method (22). The phylogenetic ANOVA was
36
37 199 implemented via the phytools package in R (23). Both morphometric and
38
39 200 performance phylogenetic ANOVAs were calculated with 10,000 simulations. To
40
41 201 elucidate differences between groups, a pairwise posthoc test was performed using
42
43 202 a Holm correction.

44
45 203

46
47 204 *Computational Fluid Dynamics*

48
49 205

1
2
3 206 To simulate flow over the beak and head, a virtual flume was simulated using
4
5 207 Autodesk CFD 2019. Digital models of *Ceyx*, *Dacelo*, and *Ceryle*, were used as
6
7
8 208 representative taxa; two attributed to terrestrial and one to aquatic feeding
9
10 209 strategies. To create suitable, watertight meshes for CFD, the scan data was
11
12 210 manipulated via a combination of Autodesk Maya 2019 and Autodesk Meshmixer.
13
14 211 First, models were aligned to world axes (anterior aligned to +x, dorsal to +y, and
15
16 212 right-lateral aligned to +z), and scaled such that beak length equaled 9 cm in all
17
18 213 specimens, so as to match the physical models used above and to remove size
19
20 214 effects. Models were then cropped posterior to the beak, but anterior to the eye
21
22 215 sockets, before holes were filled, and the models made solid. A smoothing pass was
23
24 216 applied to remove erroneous spikes in the laser scan data, or to remove small sharp
25
26 217 topography caused by errant feathers when the specimens were scanned. To avoid
27
28 218 flow artefacts from a flat surface at the back of the head, the filled surface was
29
30 219 extruded, and then deformed into a cone-shape consistent with the edges of the
31
32 220 head (Figure 5a). This avoided any abrupt or complex transitions from laser scan to
33
34 221 reconstructed posterior. The now watertight meshes were then downsampled
35
36 222 using InstantMeshes (<https://github.com/wjakob/instant-meshes> (24)) to ~20,000
37
38 223 triangles (figure 5A & B).

39
40 224 The downsampled meshes were imported into Autodesk CFD 2019, where
41
42 225 simulations were constructed in a similar manner to (25). A fluid volume was
43
44 226 generated around the mesh, so as to create a virtual flume with walls sufficiently far
45
46 227 from the mesh to avoid edge effects. Using standard materials in Autodesk CFD,
47
48 228 properties of fresh water (density = 998.2 kgm^{-3} , Viscosity = $0.001003 \text{ Pa}\cdot\text{s}$) were
49
50
51
52
53
54
55
56
57
58
59
60

1
2
3 229 applied to the fluid volume. Kingfisher models were given properties of ABS
4
5 230 Polycarbonate, though as the models were stationary and mass-less, the material
6
7
8 231 properties of the kingfisher beaks had little to no impact on results. The anterior
9
10 232 end of the flume was set as an input flow of 5ms^{-1} , approximately the same as for the
11
12 233 physical simulations. A zero-pressure boundary condition was applied to the
13
14
15 234 opposing, posterior end allowing flow through the flume at a uniform 5ms^{-1} . All
16
17 235 other fluid boundaries were set to a slip/symmetry condition. Gravity was not
18
19 236 included in the simulation. Meshing of the domain was carried out automatically
20
21 237 prior to the simulation process (Figure 5C). A steady-state simulation was run until
22
23 238 convergence, utilizing the SST k-Omega turbulence model. Results were calculated
24
25 239 and visualized using Paraview 5.6, and are presented vertically for consistency with
26
27 240 physical simulations above. We also calculated coefficient of drag: $C_d = 2F / \rho v^2 a^2$,
28
29 241 where $\rho = 998.78$, v^2 is velocity, and a^2 is cross-sectional area at the widest point of
30
31 242 the model.
32
33
34
35
36 243

38 244 **RESULTS**

43 246 *Morphology*

45 247 Diving, terrestrial, and both foraging groups differ significantly in beak
46
47 248 morphology, but these results are confounded by phylogeny for beak length and
48
49 249 depth.

52 250 After adjusting for body size, beak length differs between foraging groups
53
54
55 251 (Fig. 6A; ANOVA $F_{2,68}=13.67$, $p<0.001$). Aquatic foraging kingfishers have longer

1
2
3 252 beaks than terrestrial kingfishers (Tukey HSD $p < 0.001$), but aquatic foragers do not
4
5 253 differ from birds that forage in both ($p = 0.99$). Terrestrial kingfishers have shorter
6
7 254 beaks than birds found in the 'both' category ($p = 0.003$). These relationships are
8
9 255 confounded by phylogeny – foraging guilds are not statistically significantly
10
11 256 different in beak length (Phylogenetic ANOVA $F = 13.67$, $p = 0.14$).

12
13
14
15 257 Size-corrected beak depth differs significantly between foraging groups (Fig.
16
17 258 6B; ANOVA $F_{2,68} = 8.98$, $p < 0.001$). Aquatic foraging birds have shallower bills than
18
19 259 terrestrial ($p < 0.001$) and both ($p = 0.003$) foraging groups, but terrestrial birds do
20
21 260 not differ from birds that forage both ways ($p = 0.64$). These significances are not
22
23 261 resilient to phylogeny (Phylogenetic ANOVA $F = 8.79$, $p = 0.255$).

24
25
26
27 262 Lastly, size-corrected beak width differs between foraging groups (Fig. 6C;
28
29 263 ANOVA $F_{2,68} = 48.97$, $p < 0.001$). Aquatic beaks are narrower than terrestrial
30
31 264 ($p < 0.001$) and both ($p < 0.001$) groups. Terrestrial beaks do not differ significantly
32
33 265 from birds that forage in both methods ($p = 0.944$). After accounting for phylogenetic
34
35 266 relatedness, beak width remains significantly different between groups
36
37 267 (phylogenetic ANOVA $F = 48.97$; $p < 0.001$). Aquatic beaks remain significantly more
38
39 268 narrow than terrestrial (pairwise phylogenetically corrected $p < 0.001$) and mixed
40
41 269 ($p = 0.003$) foraging groups. Terrestrial species do not differ significantly from birds
42
43 270 that forage both aquatic and terrestrially ($p = 0.79$).

44
45
46
47 271

48
49
50 272

51
52 273 *Performance – physical simulations*
53
54
55
56
57
58
59
60

1
2
3 274 Beaks from aquatic foraging species exhibited lower average peak
4
5 275 decelerations during water entry than both terrestrial and aquatic-terrestrial
6
7
8 276 foraging species (Figure 7; ANOVA $F_{28,2}=7.645$, $p=0.002$). Aquatic and terrestrially
9
10 277 foraging species dive deceleration were significantly different (Tukey HSD,
11
12 278 $p=0.002$), while aquatic ($p=0.92$) and terrestrial ($p=0.92$) were not significantly
13
14 279 different from foraging strategies that utilized both aquatic and terrestrial styles.

15
16
17 280 When phylogeny was accounted for, the difference in performance between
18
19 281 foraging guilds remains significant (phylogenetic ANOVA, $F=7.64$, $p=0.047$).
20
21
22 282 However, a pairwise posthoc test with a Holm correction (26) found marginal
23
24 283 differences between aquatic and terrestrial foraging groups ($p=0.084$), terrestrial
25
26 284 and both foraging groups ($p=0.084$), and no difference between aquatic and both
27
28 285 foraging groups ($p=0.78$).

29
30
31 286

32 33 287 *Performance – CFD*

34
35
36 288 The CFD simulations indicate a higher anterior-posterior drag force in the
37
38 289 terrestrially foraging taxa, *Ceyx erithaca* and *Dacelo novaeguineae* than the aquatic
39
40 290 forager *Ceryle rudis*. However, while this drag force was particularly high in *Dacelo*
41
42 291 (6.86N , $C_d = 0.23$), the terrestrial *Ceyx* (2.98 N , $C_d = 0.17$) experienced only slightly
43
44 292 more drag force than the aquatic *Ceryle* (2.27 N , $C_d = 0.23$). The three simulated
45
46 293 kingfishers also exhibited differences in dorso-ventral drag force, *Dacelo* and *Ceyx*
47
48 294 both experience force in the negative horizontal direction (i.e. force pushing the
49
50 295 head ventrally) of 1.54 N and 0.68 N respectively. The aquatic foraging *Ceryle*
51
52
53 296 however, experienced 0.14 N of force in a positive horizontal direction (i.e. a force
54
55
56
57
58
59
60

1
2
3 297 acting to lift the head). Lateral forces were generally low, as would be expected, but
4
5
6 298 were not zero due to asymmetries in the scan data.

7
8 299 Visualization of fluid velocity indicates that anterior to the head, at the
9
10 300 posterior beak, is where most fluid is pushed forwards, generating pressure (or
11
12 301 form) drag. The bow waves are smallest in *Ceryle*, and then *Ceyx*, extending only a
13
14
15 302 limited distance in front of the beak. The *Dacelo* model produces a significant bow-
16
17 303 wave approximately twice the magnitude of the other models. This is most notable
18
19 304 in the extensive areas of water being pushed forwards in front of the tip of the beak
20
21
22 305 (Figure 8).

23
24 306

25
26 307

27 308 **DISCUSSION**

28
29 309

30
31
32
33 310 Our data shows that diving kingfishers have morphological adaptations
34
35 311 associated with aquatic foraging. Further, aquatic foraging species beak shapes
36
37 312 produce less hydrodynamic drag than terrestrial species, measured as lower peak
38
39 313 deceleration during impact with the water, and as drag force in CFD simulations.
40
41 314 Collectively, we find evidence that supports adaptations for improved diving
42
43 315 performance in aquatically foraging kingfishers relative to terrestrial and mixed
44
45 316 foraging species. While the exact values for deceleration and drag of our models
46
47
48 317 have been normalized to size and are therefore not directly applicable to individual
49
50 318 taxa, they do provide valuable relative information regarding potential selection for
51
52
53 319 drag-reducing shape.
54
55
56
57
58
59
60

1
2
3 320 Beak width in aquatically foraging species is less than in terrestrially foraging
4
5 321 species. Both length and depth also differ between foraging groups, but these
6
7
8 322 patterns were not significant once phylogeny was taken in to consideration. Our
9
10 323 study aligns with hydrodynamic expectations based on water piercing studies using
11
12 324 geometrically perfect cones (12, 14). Diving species have beaks of lower base width,
13
14
15 325 and tend toward longer beaks with lower base depth. (Figure 6). Additional
16
17 326 morphological details not measured in this study likely contribute to dive
18
19 327 performance, including the morphology of the head, body and wings of the bird. In
20
21
22 328 Vincent et al.'s (14) recent work, the larger the radius of the cone base (r ,
23
24 329 corresponding to depth and width on our kingfishers), the higher the initial impact
25
26 330 forces, due to increased frontal and surface area (12), which increase both pressure
27
28 331 and friction drag respectively. This suggests that not only the shape of the beak, but
29
30
31 332 the shape of the frontal area of the bird (which is generally wider than the beak)
32
33 333 likely plays a role in plunge diving. Our CFD analyses demonstrate that it is the rapid
34
35 334 increase of frontal area at the beak-head transition that generates the largest drag
36
37 335 forces, and this transition is smoothest in the diving species *Ceryle rudis* relative to
38
39 336 terrestrial species – where a larger volume of water is accelerated in the direction of
40
41
42 337 travel by the beak-head transition (Figure 8).

43
44
45 338 Our CFD models were similar, but not entirely in agreement with our
46
47 339 physical experiments. *Dacelo novaeguineae*'s physical model dive force was 107%
48
49 340 that of the CFD model (physical model = 7.4 vs. CFD = 6.9 N), *Ceyx erithaca* was
50
51 341 142% (4.2 vs. 2.3), and *Ceryle rudis* was 159% (3.6 vs. 2.3). Our CFD analysis was
52
53 342 performed on models with hydrodynamically smoothed ends, unlike the physical
54
55
56
57
58
59
60

1
2
3 343 models mounted to a pole and accelerometer, and were also tested at slightly
4
5 344 different velocities (4.5 physical models vs. 5 ms⁻¹ CFD). Most notably, the CFD was
6
7 345 performed in a closed boundary, simulating movement within water, rather than
8
9 346 transitioning between low density (air) and high density (water) fluid. The
10
11 347 mechanics of such transitions are complex (14), including cavitation and splash, and
12
13 348 are thus difficult to simulate. Thus, our CFD is likely not a precise measure of the
14
15 349 initial water entry phase, but is useful for comparing general hydrodynamic form
16
17 350 between taxa.

21
22 351 Notably, no apparent bow wave, where water is pushed forward in front of
23
24 352 the animal (27, 28) appears at the tip of the *Ceyx* or *Ceryle* kingfisher bills in the CFD
25
26 353 simulations (Figure 8A, B). However, a noticeable bow wave does appear at the
27
28 354 beak-head joint (Figure 8C). The elongated beaks of diving birds, coupled with
29
30 355 apparent beak-head streamlined morphologies, may delay the effects of this bow
31
32 356 wave long enough to avoid detection by the prey. The larger, highly terrestrial
33
34 357 forager, *Dacelo* displayed significantly greater bow waves, both in front of the beak-
35
36 358 head joint, and even in front of the beak tip, which is broader and deeper than the
37
38 359 other two taxa simulated.

42
43 360 Of interest are the resulting dorso-ventral drag forces in our CFD results
44
45 361 produced by each beak, with the terrestrial forms *Ceyx* and *Dacelo* generating forces
46
47 362 that push the head ventrally. *Ceryle*, meanwhile, generated only very small dorso-
48
49 363 ventral forces, acting in the opposite direction. This may be the result of the more
50
51 364 curved beak, in comparison with the straighter beaks of the other two models. The
52
53 365 lower forces acting orthogonal to the direction of movement may be necessary for
54
55
56
57
58
59
60

1
2
3 366 the bird to travel straight when diving into the water. Reducing these dorso-ventral
4
5 367 forces may be more important during diving, in a more viscous fluid, than in flight
6
7
8 368 through air.

9
10 369 Further work examining the hydrodynamics of living birds may illuminate
11
12 370 additional patterns. For example, our study examined only kingfisher dives with
13
14
15 371 closed beaks, with particular interest at the air-water boundary. However, the
16
17 372 kingfisher must open the bill to catch prey. At that point, the hydrodynamics of the
18
19
20 373 bird are likely to be very different. Computational fluid dynamic modeling of
21
22 374 aquatic striking snakes suggests that prey could become dislodged by a bow wave
23
24 375 created by the open jaw of the snake (27). However, the shape of the kingfisher bill,
25
26 376 particularly in aquatic foragers, is much longer, and would likely open to a lesser
27
28
29 377 angle, than a striking snake, which may reduce any emergent bow-wave. CFD
30
31 378 models in aquatic snakes suggest that larger prey sizes can offset the bow wave
32
33 379 induced movements of the prey. Behavioral studies have shown that captive Pied
34
35
36 380 kingfishers tend to select the larger available prey items (29), and the Common
37
38 381 kingfisher selects prey within a discrete size range of 5 to 6 cm in length (30). This
39
40
41 382 size selection may impede the hydrodynamic effects of displacement from the open
42
43 383 bill. Size selection could also be due to prey availability, depth (31), or visual
44
45 384 limitations, such as contrast or light refraction (32), during foraging.

46
47
48 385 Selection may act not only on the beak, but the entire frontal area of diving
49
50 386 birds. Unlike the plunge diving gannets and terns, the kingfisher neck is noticeably
51
52 387 shorter and the feathers appear to smoothly taper from the head to the body in the
53
54
55 388 dive posture – potentially ensuring an entirely streamlined body. Further work

1
2
3 389 examining entire body morphology in live animals is necessary to better understand
4
5 390 the potential for streamlining across species.
6
7

8 391 While we adjusted the overall shape of the models in order to test questions
9
10 392 pertaining to shape, not size, we can use our deceleration values to estimate if the
11
12 393 dive itself is enough to overcome buoyancy with a rough calculation. Buoyancy (N)
13
14 394 is calculated as $F_b = \rho * V_{\text{bird}} * g$, where ρ is the change between air and water density
15
16 395 (998.78 kg m^{-3}), V_{bird} is the volume of water displaced by the bird (i.e., the volume of
17
18 396 the bird, m^3), and g is gravity (9.81 m s^{-2}). As a rough estimate, we can consider a
19
20 397 spherical bird with a radius of 6 cm, which would have a buoyancy force of 2.1 N
21
22 398 that must be overcome to submerge the bird. Our prints were scaled to the beak
23
24 399 length of the largest species in the sample, the diving bird *Megaceryle maxima*,
25
26 400 which weighs 325 grams and had a deceleration value of 7.36 m s^{-2} . By $F = m a$, the
27
28 401 impact force of the bird would be 2.392 N, - a force larger than the estimated
29
30 402 buoyancy of our spherical bird, allowing total submergence. In contrast, the smallest
31
32 403 diving species, *Alcedo pusilla*, has a mass of 13.3 grams, and had a deceleration value
33
34 404 of 5.95 m s^{-2} , resulting in an impact force of 0.43 N – not enough to overcome
35
36 405 buoyancy for a 6 cm radius bird. Our calculation of buoyancy force is very rough,
37
38 406 and does not account for the density of the animal or actual volumes. Diving species
39
40 407 may be less buoyant than their terrestrial counterparts in part due to differences in
41
42 408 body mass and ability to retain air under feathers (5, 33, 34), although this has not
43
44 409 been tested in kingfishers. Birds can actively adjust their buoyancy by changing the
45
46 410 amount of air stored in the respiratory system during a dive (35). Birds may use leg-

1
2
3 411 or wing-produced thrust to help counter buoyancy during a dive following initial
4
5 412 submergence (36, 37).
6

7
8 413 Conflicting evolutionary demands are placed on beaks. For example, higher
9
10 414 mechanical advantage in relation to more leaf-based diets appears to be a primary
11
12 415 driver of beak shape in *Anseriformes* (38). Shape changes associated with increased
13
14 416 bite force in the beaks of Darwin's finches also limit the use of the jaw during song
15
16 417 production (39). Thus, it is important to keep in mind that the beak shapes tested
17
18 418 here are likely also under selection for other behaviors, including bite force, burrow
19
20 419 excavation, or territorial defense. Additionally, morphological variables not
21
22 420 measured here likely contribute to aquatic diving performance, including beak
23
24 421 surface structure (40) and position of the nares.
25
26
27
28

29 422

30
31 423 In conclusion, we showed that diving kingfishers have narrower beaks, and a
32
33 424 tendency toward longer and more shallow beaks once phylogeny is accounted for
34
35 425 when comparing to terrestrial species. Our physical simulations show that diving
36
37 426 species beak shapes experience markedly less deceleration when entering the
38
39 427 water, corroborated by CFD models. This repeated evolution of functionally and
40
41 428 morphologically more hydrodynamic beaks across the kingfisher phylogeny
42
43 429 suggests convergence on morphology to improve foraging success in diving birds.
44
45 430 Our work may help further inspire engineering solutions, including robotics
46
47 431 working at the air-water interface.
48
49
50

51 432

52 433

53 434

54 435

55

56

57

58

59

60

1
2
3 436 **AUTHOR'S CONTRIBUTIONS**

4 437
5 438 KEC conceived of the study. KEC, ROH, and PLF contributed to the design of the
6 439 study and drafting the manuscript. KEC and ROH acquired the data for the physical
7 440 tests and performed statistical analyses, PLF carried out computational fluid
8 441 dynamics analyses. All authors gave final approval for publication and agree to be
9 442 held accountable for all aspects of the work.
10 443

11 444

12 445

13 446
14 447 **ACKNOWLEDGEMENTS**

15 448

16 449 The authors extend a sincere thank you to Chris Cooney, Gavin Thomas, and the
17 450 MarkMyBird.org team at Sheffield University for the generous access to the digital
18 451 3D models of most of the birds used in this study. We subsequently thank the
19 452 Manchester Museum, Brambell Museum at Bangor University, and the Natural
20 453 History Museum at Tring for access to original specimens. We also thank the
21 454 FabLab Pontio Innovation Centre at Bangor University for training, assistance, and
22 455 access to laser scanning and 3D printing technologies: Wyn Griffith, John Story, and
23 456 Sara Roberts. This manuscript was improved thanks to discussions at the 2018
24 457 London regional SICB DVM meeting with Dr. Jim Usherwood (who suggested
25 458 modelling buoyancy) and Dr Sam Van Wassenbergh at the 2019 SICB annual
26 459 meeting. PLF would like to thank Dr Pernille Troelsen for useful discussions
27 460 regarding CFD software. The authors also wish to thank Charlotte Cannon for
28 461 assistance with experiments, and Charles Bishop and Tom Brekke for helpful
29 462 discussions.
30 463

31 464

32 465

33 466

34 467

35 468

36 469

37 470

38 471

39 472

40 473

41 474

42 475

43 476

44 477

45 478

46 479

47 480

48 481

49 482

50 483

51 484

52 485

53 486

54 487

55 488

56 489

57 490

58 491

59 492

60 493

462 **DATA ACCESSIBILITY**

464 Data is available as a supplemental file.

466 **FUNDING STATEMENT**

468 KEC is funded by a Leverhulme Early Career Fellowship.

471 **REFERENCES**

- 472 1. Wolpert H. Engineered Biomimicry: The World's Top Olympians: Elsevier
473 Inc. Chapters; 2013.
- 474 2. Foo CT, Omar B, Taib I, editors. Shape Optimization of High-Speed Rail by
475 Biomimetic. MATEC Web of Conferences; 2017: EDP Sciences.
- 476 3. Ropert-Coudert Y, Grémillet D, Ryan P, Kato A, Naito Y, Le Maho Y. Between
477 air and water: the plunge dive of the Cape Gannet *Morus capensis*. Ibis.
478 2004;146(2):281-90.

1
2
3
4
5
6
7
8
9
10
11
12
13
14
15
16
17
18
19
20
21
22
23
24
25
26
27
28
29
30
31
32
33
34
35
36
37
38
39
40
41
42
43
44
45
46
47
48
49
50
51
52
53
54
55
56
57
58
59
60

- 479 4. Stephenson R. Diving energetics in lesser scaup (*Aythya affinis*, Eyton).
480 Journal of Experimental Biology. 1994;190(1):155-78.
- 481 5. Lovvorn JR, Jones DR. Effects of body size, body fat, and change in pressure
482 with depth on buoyancy and costs of diving in ducks (*Aythya spp.*).
483 Canadian Journal of Zoology. 1991;69(11):2879-87.
- 484 6. Stephenson R, Lovvorn J, Heieis M, Jones D, Blake R. A hydromechanical
485 estimate of the power requirements of diving and surface swimming in
486 lesser scaup (*Aythya affinis*). Journal of Experimental biology.
487 1989;147(1):507-18.
- 488 7. Hedenstrom A, Liechti F. Field estimates of body drag coefficient on the
489 basis of dives in passerine birds. Journal of Experimental Biology.
490 2001;204(6):1167-75.
- 491 8. Feldkamp SD. Swimming in the California sea lion: morphometrics, drag
492 and energetics. Journal of Experimental Biology. 1987;131(1):117-35.
- 493 9. Bannasch R. Drag minimisation on bodies of revolution in nature and
494 engineering. 1993.
- 495 10. Bannasch R. Hydrodynamics of penguins-an experimental approach.
496 1995;Advances in Penguin Biology:141-76.
- 497 11. Lovvorn J, Liggins GA, Borstad MH, Calisal SM, Mikkelsen J. Hydrodynamic
498 drag of diving birds: effects of body size, body shape and feathers at steady
499 speeds. Journal of Experimental Biology. 2001;204(9):1547-57.
- 500 12. Chang B, Croson M, Straker L, Gart S, Dove C, Gerwin J, et al. How seabirds
501 plunge-dive without injuries. Proceedings of the National Academy of
502 Sciences. 2016;113(43):12006-11.
- 503 13. Katzir G, Camhi JM. Escape response of black mollies (*Poecilia sphenops*) to
504 predatory dives of a pied kingfisher (*Ceryle rudis*). Copeia.
505 1993;1993(2):549-53.
- 506 14. Vincent L, Xiao T, Yohann D, Jung S, Kanso E. Dynamics of water entry.
507 Journal of Fluid Mechanics. 2018;846:508-35.
- 508 15. Fry CH, Fry K. Kingfishers, bee-eaters and rollers: A&C Black; 2010.
- 509 16. Cooney CR, Bright JA, Capp EJ, Chira AM, Hughes EC, Moody CJ. Mega-
510 evolutionary dynamics of the adaptive radiation of birds. Nature.
511 2017;542(7641):344.
- 512 17. Dunning Jr JB. CRC handbook of avian body masses: CRC press; 2007.
- 513 18. del Hoyo J, Elliot A, Sargatal J, Christie D, de Juana E. Handbook of the Birds
514 of the World Alive. Barcelona: Lynx Edicions; 2018
- 515 19. Andersen MJ, McCullough JM, Mauck III WM, Smith BT, Moyle RG. A
516 phylogeny of kingfishers reveals an Indomalayan origin and elevated rates
517 of diversification on oceanic islands. Journal of Biogeography.
518 2018;45(2):269-81.
- 519 20. Jetz W, Thomas G, Joy J, Hartmann K, Mooers A. The global diversity of birds
520 in space and time. Nature. 2012;491(7424):444.
- 521 21. Grafen A. The phylogenetic regression. Phil Trans R Soc Lond B.
522 1989;326(1233):119-57.

- 1
2
3 523 22. Garland Jr T, Dickerman AW, Janis CM, Jones JA. Phylogenetic analysis of
4 524 covariance by computer simulation. *Systematic Biology*. 1993;42(3):265-
5 525 92.
6 526 23. Revell LJ. phytools: an R package for phylogenetic comparative biology
7 527 (and other things). *Methods in Ecology & Evolution*. 2012;3(2):217-23.
8 528 24. Jakob W, Tarini M, Panozzo D, Sorkine-Hornung O. Instant field-aligned
9 529 meshes. *ACM Transactions on Graphics (Proceedings of SIGGRAPH Asia*
10 530 *2015)*. 2015;34(6):189:1-:15.
11 531 25. Troelsen P, Wilkinson D, Seddighi M, Allanson D, Falkingham P. Functional
12 532 morphology and hydrodynamics of plesiosaur necks: Does size matter?
13 533 *Journal of Vertebrate Paleontology*. in press.
14 534 26. Holm S. A simple sequentially rejective multiple test procedure.
15 535 *Scandinavian journal of statistics*. 1979:65-70.
16 536 27. Van Wassenbergh S, Brecko J, Aerts P, Stouten I, Vanheusden G, Camps A, et
17 537 al. Hydrodynamic constraints on prey-capture performance in forward-
18 538 striking snakes. *Journal of the Royal Society Interface*. 2009:rsif20090385.
19 539 28. Herrel A, Vincent S, Alfaro M, Van Wassenbergh S, Vanhooydonck B,
20 540 Irschick D. Morphological convergence as a consequence of extreme
21 541 functional demands: examples from the feeding system of natricine snakes.
22 542 *Journal of evolutionary biology*. 2008;21(5):1438-48.
23 543 29. Labinger Z, Katzir G, Benjamini Y. Prey size choice by captive pied
24 544 kingfishers, *Ceryle rudis* L. *Animal behaviour*. 1991;42(6):969-75.
25 545 30. Vilches A, Miranda R, Arizaga J. Fish prey selection by the Common
26 546 Kingfisher *Alcedo atthis* in Northern Iberia. *Acta ornithologica*.
27 547 2012;47(2):167-75.
28 548 31. Vilches A, Arizaga J, Salvo I, Miranda R. An experimental evaluation of the
29 549 influence of water depth and bottom color on the common kingfisher's
30 550 foraging performance. *Behavioural processes*. 2013;98:25-30.
31 551 32. Katzir G, Lotem A, Intrator N. Stationary underwater prey missed by reef
32 552 herons, *Egretta gularis*: head position and light refraction at the moment of
33 553 strike. *Journal of Comparative Physiology A*. 1989;165(4):573-6.
34 554 33. Dove CJ, Agreda A. Differences in plumulaceous feather characters of
35 555 dabbling and diving ducks. *Condor*. 2007:192-9.
36 556 34. Lovvorn JR, Jones DR. Biomechanical conflicts between adaptations for
37 557 diving and aerial flight in estuarine birds. *Estuaries*. 1994;17(1):62.
38 558 35. Sato K, Naito Y, Kato A, Niizuma Y, Watanuki Y, Charrassin J, et al. Buoyancy
39 559 and maximal diving depth in penguins: do they control inhaling air volume?
40 560 *Journal of Experimental Biology*. 2002;205(9):1189-97.
41 561 36. Ribak G, Weihs D, Arad Z. How do cormorants counter buoyancy during
42 562 submerged swimming? *Journal of Experimental Biology*.
43 563 2004;207(12):2101-14.
44 564 37. Clifton GT, Biewener AA. Foot-propelled swimming kinematics and turning
45 565 strategies in common loons. *Journal of Experimental Biology*.
46 566 2018;221(19):jeb168831.
47 567 38. Olsen AM. Feeding ecology is the primary driver of beak shape
48 568 diversification in waterfowl. *Functional Ecology*. 2017;31(10):1985-95.

- 1
2
3 569 39. Herrel A, Podos J, Vanhooydonck B, Hendry A. Force-velocity trade-off in
4 570 Darwin's finch jaw function: a biomechanical basis for ecological
5 571 speciation? *Functional Ecology*. 2009;23(1):119-25.
6 572 40. Martin S, Bhushan B. Discovery of riblets in a bird beak (Rynchops) for low
7 573 fluid drag. *J Phil Trans R Soc A*. 2016;374(2073):20160134.
8 574
9

10
11 575

12 576 **FIGURE LEGENDS**

13 577

14 578 **Figure 1:** The phylogeny of 71 kingfishers (Alcedinidae) used for morphometric
15 579 analysis in this study, constructed as a sub-sample of Anderson et al. (2018).
16 580 Coloured circles represent classified foraging group: blue are aquatic foraging
17 581 (diving) species, grey are mixed (aquatic and terrestrial), and green are terrestrially
18 582 foraging species. See text for details.
19 583

20 584

21 585 **Figure 2:** Morphometric variables collected for each species on the Common
22 586 Kingfisher, *Alcedo atthis*. (A) Lateral view, (B) Dorsal view. Beak Length
23 587 measurements were scaled to 9 cm in all 3D models to standardize for body size.
24 588 See text for additional details.

25 589

26 590 **Figure 3:** Phylogeny of 31 species of kingfishers used for performance testing,
27 591 subsampled from the phylogeny in figure (1) (Anderson et al. 2018). Coloured
28 592 circles represent classified foraging group: blue are aquatic foraging (diving)
29 593 species, grey are mixed (aquatic and terrestrial), and green are terrestrially foraging
30 594 species.

31 595

32 596 **Figure 4: (A)** Diagram of diving tank set up. Dive tank was 60 cm tall with an
33 597 opening of 25 cm. The dive body consists of a 50 ml falcon tube containing the
34 598 accelerometer and additional weights as needed. The accelerometer was mounted
35 599 with the negative x-axis aligned with gravity, and the positive z axis oriented
36 600 perpendicular to the bird dorsally. The falcon tube was fitted with plastic drinking
37 601 straws on either side, and the straws were threaded along fishing line to maintain
38 602 the dive orientation perpendicular to the water surface. **(B)** Exemplar
39 603 accelerometer data from three representative species: *Ceryle rudis* (pied kingfisher),
40 604 *Dacelo novaeguineae* (Laughing Kookaburra), and *Ceyx erithaca* (Black backed
41 605 kingfisher). Data is smoothed by taking a running average for 3 points, and is
42 606 truncated before cavitation.

43 607

44 608 **Figure 5:** Kingfisher beak models and CFD domain. **(A)** Original scan data (above),
45 609 and cleaned, smoothed, and scaled model (below) of *Ceryle* presented in lateral and
46 610 posterior-lateral views. Models were cropped at the posterior most portion of the
47 611 beak, then holes were filled, surfaces extruded, and final model then smoothed. **(B)**
48 612 Original and cleaned meshes for *Ceyx*, *Ceryle*, and *Dacelo*, left to right. Grid
49 613 represents 1 cm squares. **(C)** Meshed CFD domain.

50
51
52
53
54
55
56
57
58
59
60

1
2
3 614 **Figure 6: (A-C)** Residuals of morphological characters regressed against body mass,
4 615 resulting in size-corrected beak morphometrics for kingfisher species classified as
5 616 aquatic foragers (blue), mixed foragers (grey), and terrestrial foragers (green). **(D-**
6 617 **F)** Uncorrected measurements for morphological characters (in mm). Size-
7 618 corrected (A) beak length, (B), beak depth, and (C) beak width are all statistically
8 619 significantly different between foraging guilds (ANOVA $F_{2,68}=48.97$, $p < 0.001$). Once
9 620 phylogeny is accounted for, only beak width (C) remains significantly different
10 621 between size-corrected aquatic and terrestrial species (phylogenetically corrected p
11 622 < 0.001).
12 623

13 624 **Figure 7:** Average peak deceleration values measured for 3D printed scaled models
14 625 of kingfisher beaks classified as aquatic foragers (blue), mixed foragers (grey), and
15 626 terrestrially foraging species (green). Aquatic and terrestrially foraging species dive
16 627 deceleration are significantly different (ANOVA $F_{28,2}=7.645$, $p=0.002$, Tukey HSD,
17 628 $p=0.002$). This result is not affected by phylogenetic relatedness (phylogenetic
18 629 ANOVA, $F=7.64$, $p=0.047$).
19 630

20 631 **Figure 8:** Water velocity in the anterior-posterior direction in front of the head of
21 632 (A) *Ceryle*, (B) *Ceyx*, and (C) *Dacelo*. Velocity scale is truncated to illustrate areas of
22 633 high and low velocity. Note the much larger bow wave in front of the highly
23 634 terrestrial *Dacelo*. Bottom: Static pressure around (D) *Ceryle*, (E) *Ceyx*, and (F)
24 635 *Dacelo*.
25 636
26
27
28
29
30
31
32
33
34
35
36
37
38
39
40
41
42
43
44
45
46
47
48
49
50
51
52
53
54
55
56
57
58
59
60

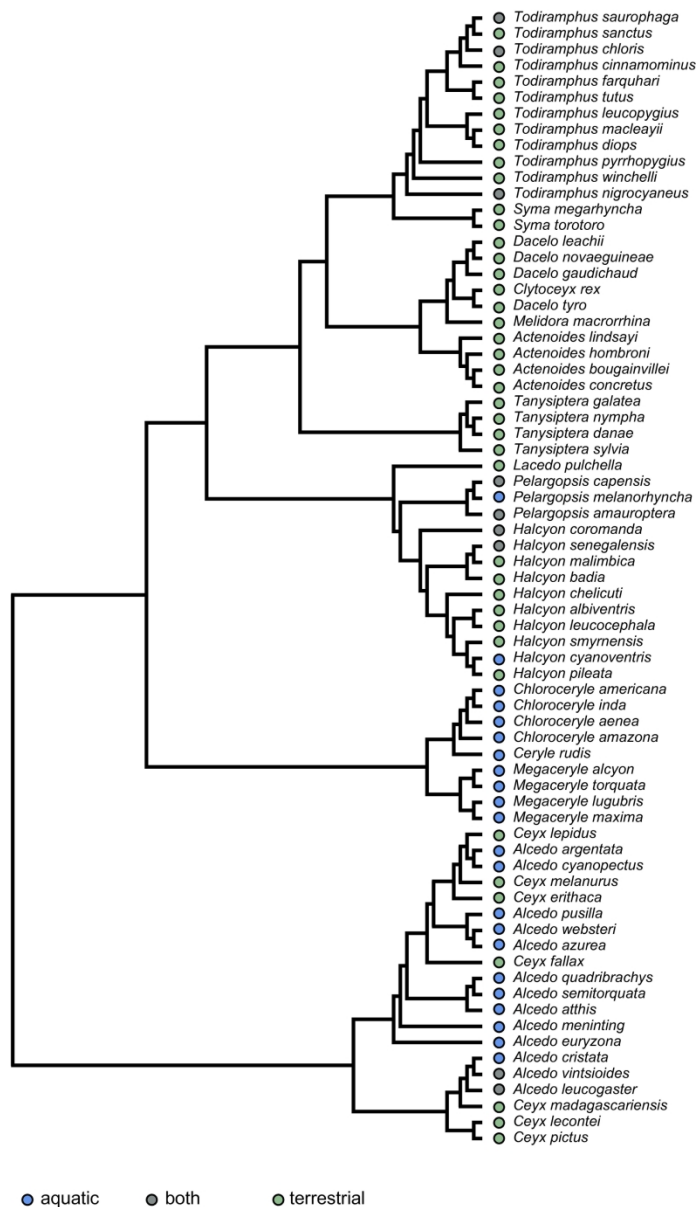
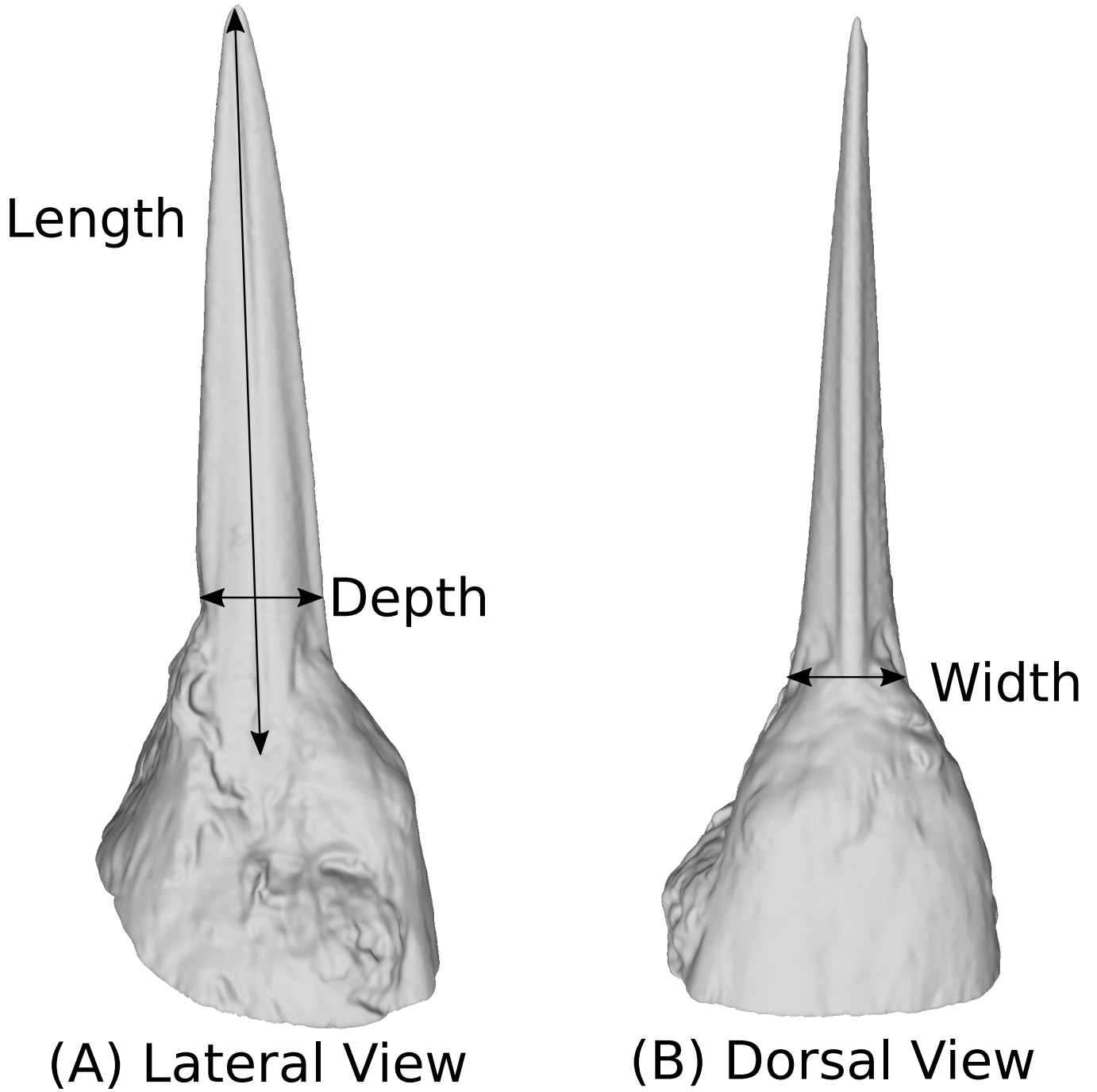
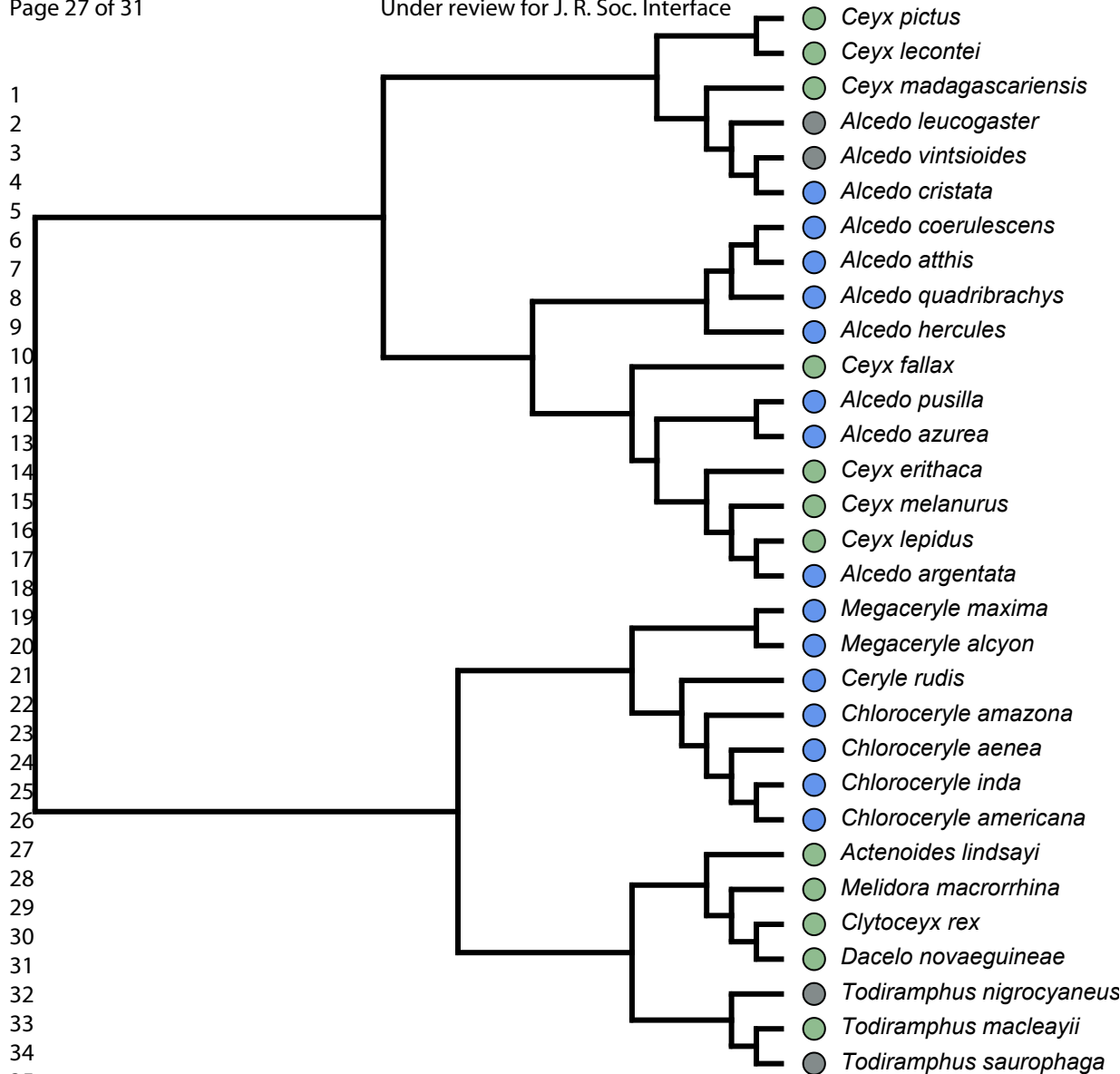
1
2
3
4
5
6
7
8
9
10
11
12
13
14
15
16
17
18
19
20
21
22
23
24
25
26
27
28
29
30
31
32
33
34
35
36
37
38
39
40
41
42
43
44
45
46
47
48
49
50
51
52
53
54
55
56
57
58
59
60

Figure 1: The phylogeny of 71 kingfishers (Alcedinidae) used for morphometric analysis in this study, constructed as a sub-sample of Anderson et al. (2018). Coloured circles represent classified foraging group: blue are aquatic foraging (diving) species, grey are mixed (aquatic and terrestrial), and green are terrestrially foraging species. See text for details.

159x279mm (300 x 300 DPI)



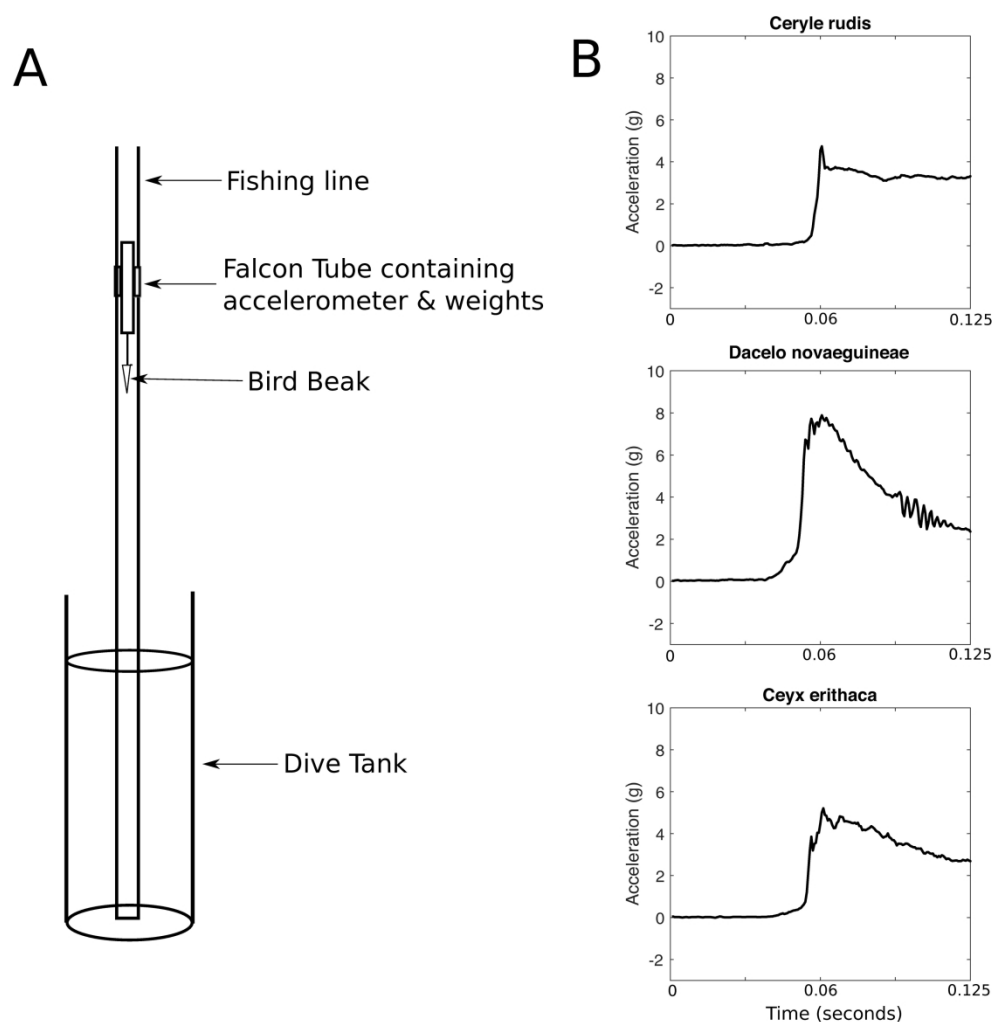
1
2
3
4
5
6
7
8
9
10
11
12
13
14
15
16
17
18
19
20
21
22
23
24
25
26
27
28
29
30
31
32
33
34
35
36
37
38
39
40
41
42
43
44
45
46
47
48
49
50
51
52
53
54
55
56
57
58
59
60



<http://mc.manuscriptcentral.com/jrsi>

37 ● aquatic ● both ● terrestrial

38



39
40
41
42
43
44
45
46

Figure 4: (A) Diagram of diving tank set up. Dive tank was 60 cm tall with an opening of 25 cm. The dive body consists of a 50 ml falcon tube containing the accelerometer and additional weights as needed. The accelerometer was mounted with the negative x-axis aligned with gravity, and the positive z axis oriented perpendicular to the bird dorsally. The falcon tube was fitted with plastic drinking straws on either side, and the straws were threaded along fishing line to maintain the dive orientation perpendicular to the water surface. (B) Exemplar accelerometer data from three representative species: *Ceryle rudis* (pied kingfisher), *Dacelo novaeguineae* (Laughing Kookaburra), and *Ceyx erithaca* (Black backed kingfisher). Data is smoothed by taking a running average for 3 points, and is truncated before cavitation.

47
48
49

275x279mm (300 x 300 DPI)

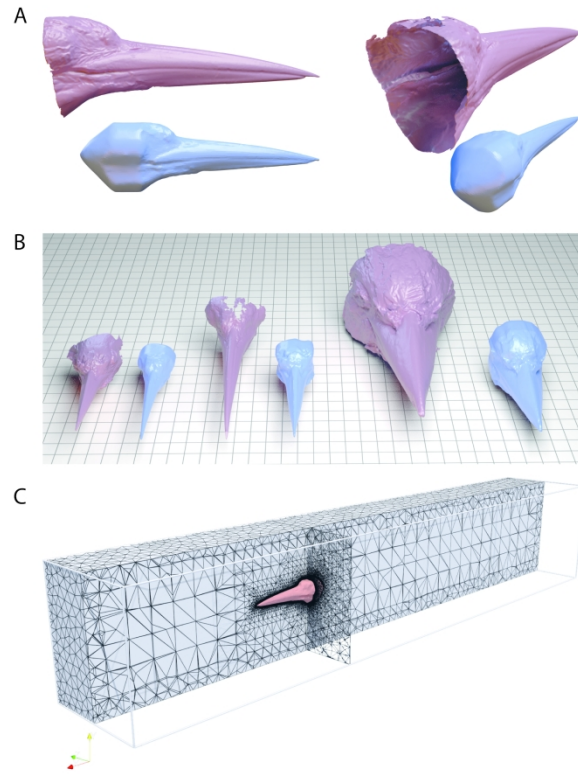


Figure 5: Kingfisher beak models and CFD domain. (A) Original scan data (above), and cleaned, smoothed, and scaled model (below) of *Ceryle* presented in lateral and posterior-lateral views. Models were cropped at the posterior most portion of the beak, then holes were filled, surfaces extruded, and final model then smoothed. (B) Original and cleaned meshes for *Ceyx*, *Ceryle*, and *Dacelo*, left to right. Grid represents 1 cm squares. (C) Meshed CFD domain.

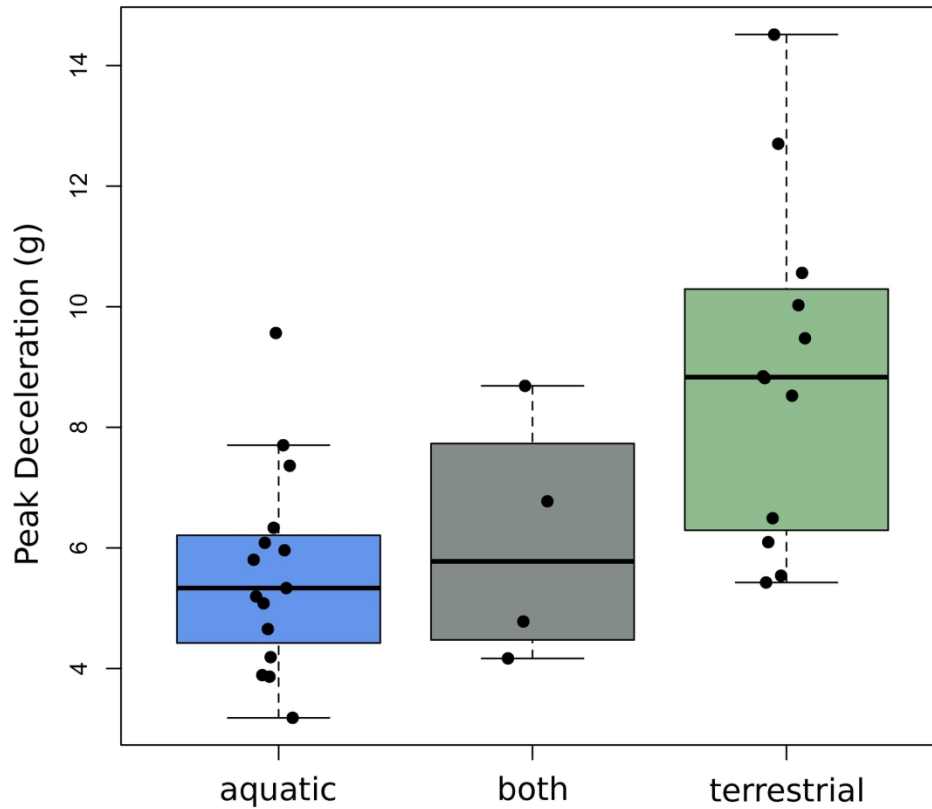


Figure 7: Average peak deceleration values measured for 3D printed scaled models of kingfisher beaks classified as aquatic foragers (blue), mixed foragers (grey), and terrestrial foragers (green). Aquatic and terrestrially foraging species dive deceleration are significantly different (ANOVA $F_{28,2}=7.645$, $p=0.002$, Tukey HSD, $p=0.002$). This result is not affected by phylogenetic relatedness (phylogenetic ANOVA, $F=7.64$, $p=0.047$).

177x177mm (300 x 300 DPI)

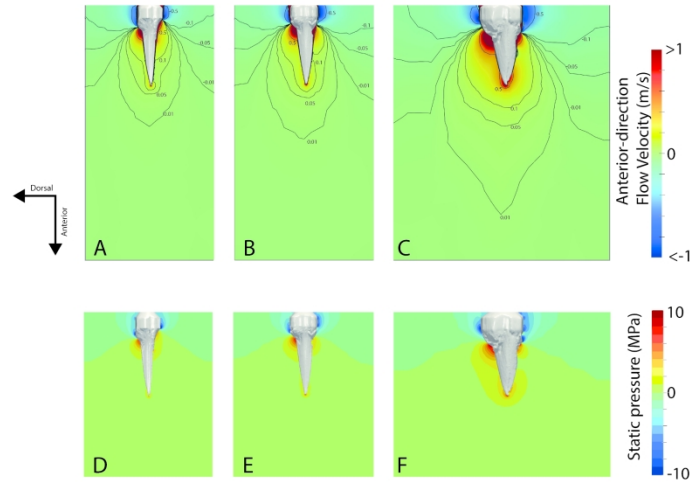


Figure 8: Water velocity in the anterior-posterior direction in front of the head of (A) Ceryle, (B) Ceyx, and (C) Dacelo. Velocity scale is truncated to illustrate areas of high and low velocity. Note the much larger bow wave in front of the highly terrestrial Dacelo. Bottom: Static pressure around (D) Ceryle, (E) Ceyx, and (F) Dacelo.